AIP | Review of Scientific Instruments

High-pressure cell for neutron reflectometry of supercritical and subcritical fluids at solid interfaces

Justin R. Carmichael, Gernot Rother, James F. Browning, John F. Ankner, Jose L. Banuelos et al.

Citation: Rev. Sci. Instrum. **83**, 045108 (2012); doi: 10.1063/1.3697999
View online: http://dx.doi.org/10.1063/1.3697999
View Table of Contents: http://rsi.aip.org/resource/1/RSINAK/v83/i4
Published by the American Institute of Physics.

Related Articles

ARGon3: "3D appearance robot-based gonioreflectometer" at PTB
Rev. Sci. Instrum. 83, 045102 (2012)

Refractive index sensor based on hybrid coupler with short-range surface plasmon polariton and dielectric waveguide
Appl. Phys. Lett. 100, 111108 (2012)

Combined ellipsometry and refractometry technique for characterisation of liquid crystal based nanocomposites
Rev. Sci. Instrum. 83, 035103 (2012)

Gas refractometry using a hollow-core photonic bandgap fiber in a Mach-Zehnder-type interferometer
Appl. Phys. Lett. 100, 051106 (2012)

Spectroscopic reflectometry of mirror surfaces during plasma exposure
Rev. Sci. Instrum. 83, 013509 (2012)

Additional information on Rev. Sci. Instrum.

Journal Homepage: http://rsi.aip.org
Journal Information: http://rsi.aip.org/about/about_the_journal
Top downloads: http://rsi.aip.org/features/most_downloaded
Information for Authors: http://rsi.aip.org/authors

ADVERTISEMENT

Downloaded 06 Apr 2012 to 128.219.49.14. Redistribution subject to AIP license or copyright; see http://rsi.aip.org/about/rights_and_permissions

High-pressure cell for neutron reflectometry of supercritical and subcritical fluids at solid interfaces

Justin R. Carmichael,[1,a)] Gernot Rother,[2,a)] James F. Browning,[1] John F. Ankner,[1] Jose L. Banuelos,[2] Lawrence M. Anovitz,[2] David J. Wesolowski,[2] and David R. Cole[2,b)]
[1]*Neutron Scattering Science Division, Oak Ridge National Laboratory, Tennessee 37831, USA*
[2]*Chemical Sciences Division, Oak Ridge National Laboratory, Tennessee 37831-6110, USA*

(Received 13 September 2011; accepted 9 March 2012; published online 6 April 2012)

A new high-pressure cell design for use in neutron reflectometry (NR) for pressures up to 50 MPa and a temperature range of 300–473 K is described. The cell design guides the neutron beam through the working crystal without passing through additional windows or the bulk fluid, which provides for a high neutron transmission, low scattering background, and low beam distortion. The o-ring seal is suitable for a wide range of subcritical and supercritical fluids and ensures high chemical and pressure stability. Wafers with a diameter of 5.08 cm (2 in.) and 5 mm or 10 mm thickness can be used with the cells, depending on the required pressure and momentum transfer range. The fluid volume in the sample cell is very small at about 0.1 ml, which minimizes scattering background and stored energy. The cell design and pressure setup for measurements with supercritical fluids are described. NR data are shown for silicon/silicon oxide and quartz wafers measured against air and subsequently within the high-pressure cell to demonstrate the neutron characteristics of the high-pressure cell. Neutron reflectivity data for supercritical CO_2 in contact with quartz and Si/SiO_2 wafers are also shown.
© *2012 American Institute of Physics*. [http://dx.doi.org/10.1063/1.3697999]

I. INTRODUCTION

Neutron reflectometry (NR) is a powerful tool to study surface and interfacial phenomena on the nanometer length scale.[1–3] Typical applications are the study of liquid-gas, liquid-liquid, gas-solid, and liquid-solid interfaces, as well as the sorption and coating of surfactants, polymers and biopolymers at these interfaces. NR can measure the neutron scattering length density profile perpendicular to a smooth interface with a resolution of ∼5–10 Å. The inherent strengths of neutron scattering experiments are the weak interaction of the neutrons with the sample (and cell), and the possibility of neutron contrast variation by, e.g., H/D isotope substitution.

The study of density profiles of pure and binary compressed fluids at solid interfaces, sorption properties of aqueous solutions of bio-macromolecules as a function of pressure, and sorption properties of species dissolved in supercritical CO_2 at solid interfaces are examples of the wide range of current research interests that require a high-pressure neutron reflectometry cell.

Subcritical and supercritical carbon dioxide is of special interest both for its potential use as a green solvent and the need to reduce its concentration in the atmosphere. Detailed knowledge of the solid-fluid interactions as a function of fluid density and temperature is important for numerous applications, including carbon storage in subsurface reservoirs and supercritical fluid chromatography. Many more fluids, including methane, propane, butane, sulfur hexafluoride, and others are studied experimentally for their environmental relevance and/or interesting physico-chemical properties like gas-liquid phase transitions in a relatively modest temperature and pressure range.

However, neutron reflectometry pressure cells that can handle these fluids have, until recently, not been readily available. A number of pressure cells exist for small-angle neutron scattering applications.[4–6] In contrast, only few NR pressure cells exist, some of which were designed for relatively low pressures.[7] High-pressure NR cells have been in use at some neutron scattering facilities. For instance, the effect of liquid and supercritical CO_2 on the swelling properties of polymers at interfaces has been studied by Watkins and co-workers[8,9] using neutron reflectometry and a pressure cell with sapphire windows. Two high-pressure neutron reflectometry cells have recently been built and employed for neutron reflectivity measurements at the Berlin Neutron Scattering Facility, where emphasis was placed on the study of sorption and film formation from aqueous solutions of polymers and lipids to solid interfaces. The cell developed by Kreuzer *et al.*,[10] which is similar in design to the cell by Koga *et al.*,[11] allows pressures of up to 100 MPa and has a sample volume of about 55 ml. The high-pressure reflectivity cell described in Jeworrek *et al.*,[12] is designed for higher pressures of up to 250 MPa and temperatures of 5–75 °C, and has a smaller sample volume of about 6 ml.

The new Oak Ridge NR pressure cell was designed with the primary goal to study the properties of supercritical CO_2 and other fluids of geochemical interest at mineral interfaces under conditions found in Earth's upper crust. Special attention was paid to the high pressure seal, as supercritical fluids have low viscosities. The cell is optimized for use at the Liquids Reflectometer located on beam line 4B (BL-4B) at the Spallation Neutron Source (SNS) at Oak Ridge National

a)Authors to whom correspondence should be addressed. Electronic addresses: carmichaeljr@ornl.gov and rotherg@ornl.gov.
b)Present address: School of Earth Sciences, The Ohio State University, Columbus, Ohio 43210, USA.

 © 2012 American Institute of Physics

Downloaded 06 Apr 2012 to 128.219.49.14. Redistribution subject to AIP license or copyright; see http://rsi.aip.org/about/rights_and_permissions

Laboratory (ORNL). The Liquids Reflectometer features a horizontal sample geometry and thus can accommodate gas/liquid surfaces in addition to gas/solid, solid/solid, and liquid/solid interfaces. Currently, reflectivities down to 5×10^{-7} can be resolved. Active vibration isolation minimizes capillary-wave production by the external environment. The data rates and Q range covered at a single scattering angle are sufficiently high to permit "real-time" kinetic studies on many systems. Time-resolved experiments include investigations of chemical kinetics, solid-state reactions, phase transitions, and chemical reactions in general.

The SNS Liquids Reflectometer is useful for a wide range of science including materials of interest in the geosciences, biomaterials, polymers, and chemistry involving thin layers of surfactants or other materials on the surfaces of liquids, such as cell-membrane analogs. The Liquids Reflectometer provides a flexible platform to study structure–property relationships at the boundary between hard and soft matter, with applications in geochemistry, biomimetics, bio-sensing, biocompatible films, hydrogen storage, and fuel cells as well as polymers.

In the high-pressure reflectometry cell described here, we employ two unique design features. First, the neutron beam passes directly through the working crystal as opposed to a conventional design with pressure bearing entrance and exit windows, which eliminates sources of neutron absorption and scattering. Second, the fluid sample volume is very small, ~0.1 ml, which reduces the scattering from the fluid (a significant advantage for hydrogen-bearing fluid species) and allows for studies of costly (e.g., deuterated) samples. While similar beam guidance designs have been used in non-pressurized neutron reflectometry cells, to our knowledge this is the first application of this design to pressure cells. A photograph of the NR pressure cell for wafers with 5 mm thickness in its assembled form is shown in Figure 1, complete with the instrument adapter plate that automatically positions the cell in the neutron beam.

FIG. 1. The high-pressure reflectometry cell in assembled state. The mantle surface of the silicon crystal (dark grey color) is visible in the center of the beam window. The 1/16 in. HIP pressure tubing connects to the internal fluid volume underneath the silicon crystal.

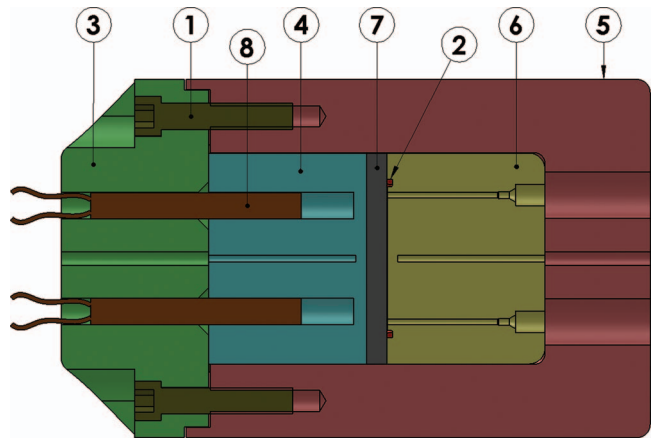

FIG. 2. Cross-sectional view of the high-pressure reflectometry cell. Labels: (1) Pressure retaining fasteners, (2) o-ring seal, (3) pressure cell cap, (4) top support cylinder, (5) high-pressure cell body, (6) titanium support cylinder, (7) wafer, and (8) heater cartridges.

II. THE HIGH-PRESSURE CELL FOR NR

The pressure cell is designed for operation at pressures from 0 to 50 MPa and temperatures from 300 to 473 K.

A labeled cross-sectional view of the cell is shown in Figure 2. The cell was designed for the commonly used wafer diameter of 2 in. (item 7). The pressurized sample space is contained in a small recessed volume (see Figure 3) between the wafer (7) and the titanium (Ti) support cylinder (6). The Ti support cylinder has entrance and exit pressure connections allowing for pressurized fluid flow through the cell, if desired. Ti was chosen for the support cylinder because of its superior corrosion resistance to a wide range of fluids at the operating temperatures of interest. A precision-machined o-ring (2) seal was incorporated to reliably contain low-viscosity supercritical fluids at elevated pressures and temperatures. The neutron beam is finely collimated so that it only passes through the wafer (single crystal wafer of silicon, sapphire, quartz, etc.). Thus, minimal neutron beam attenuation and distortion are

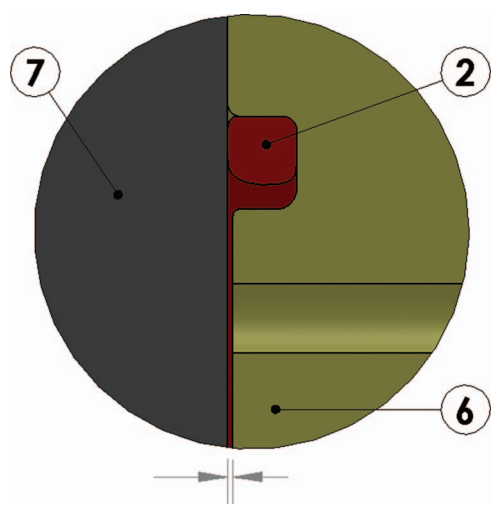

FIG. 3. Detailed cross-sectional view of the o-ring seal groove: the fluid flow channel enters the recessed sample volume behind the o-ring groove. The distance shown is ~0.1 mm. Labels: (2) o-ring seal (shown compressed), (6) titanium support cylinder, and (7) wafer.

Downloaded 06 Apr 2012 to 128.219.49.14. Redistribution subject to AIP license or copyright; see http://rsi.aip.org/about/rights_and_permissions

achieved. For instance, the beam is attenuated by less than 10% with commonly used silicon wafers. The pressurized sample acts upon both the wafer (7) and the support cylinder (6), and is contained by the o-ring (2).

Detail of the o-ring seal groove geometry is shown in Figure 3. The geometry of the groove and surface finishes were carefully selected to ensure a good seal at high pressures. All sides of the o-ring groove were highly polished to prevent leakage paths from developing in operation. The o-ring, made of 90 Shore A hardness PTFE (Parker O-Ring Compound FF202-90), remains rigid at elevated temperatures (rated to 593 K) and is resistant to chemical attack.

Compression of the o-ring seal is provided by the tightening of eight high-strength A-286 super alloy retaining fasteners (1), which transfer force through the carbon steel cap (3), and top compression cylinder (4) to the wafer (7). These retaining fasteners are also subjected to the force from the cell pressure acting over the area of the wafer. As such, it is necessary to calculate the stresses in the threads. The stress in the weaker internal threads is calculated by dividing the load per screw by the shear area of the internal thread given by

$$A_{TS} = \pi n L_e D_{s_\min}\left[\frac{1}{2n} + 0.57735(D_{s_\min} - E_{n_\max})\right], \tag{1}$$

where n is the number of threads per unit length, L_e the length of engagement, D_{s_min} the minimum major diameter of the external thread, and E_{n_max} the maximum pitch diameter of the internal thread.[13] Since the force is transmitted from the top cylinder to the wafer, the mating surfaces of both the wafer and the cylinder are polished and flat. A thin layer of PTFE film less than 25 μm thick may be placed between the contacting surfaces to prevent stress risers from surface imperfections.

The high strength carbon steel cell body (5) and cap are designed to minimize deformation at elevated pressures and temperatures in order to maintain integrity of the o-ring seal. At an internal pressure of 50 MPa, the total force in the cell acting through the upper and lower support cylinders is ~100 kN. To ensure integrity of the o-ring seal by minimizing deformations and stresses in the cell, finite element method (FEM) calculations were performed using the ABAQUS™ software package. Figure 4 shows the stresses and deflections resulting from the FEM simulation on one quadrant of the cell body (utilizing symmetry boundary conditions). The highest observed stresses occur in the radius at the bottom of the vessel insert hole where the Ti cylinder rests. Other stresses are comparatively low.

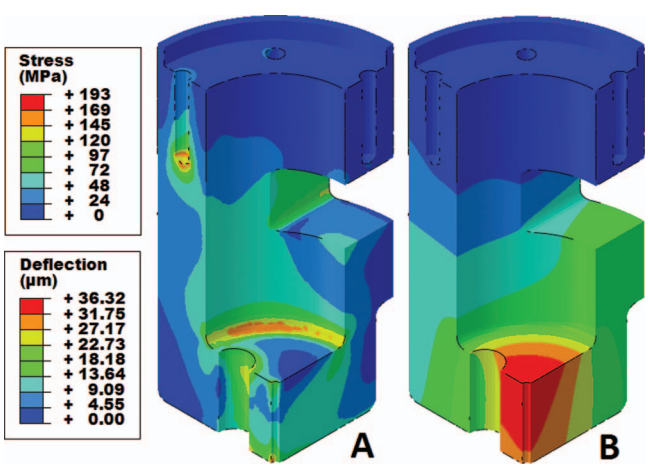

FIG. 4. FEM simulation of the pressure cell body showing von-Mises stresses (a) and deflection (b).

Each component is subject to thermal expansion and compression. Both thermal expansion of the vessel body and tension from the axial forces resulting from the pressurized fluid cause the o-ring gap to increase in length. For the two cylinders, compression from the forces also increases the length while thermal expansion helps to close the gap in the o-ring seal. This change in length can be approximated analytically by

$$\Delta L = L_0[a_L \Delta T + F/A_0 E], \tag{2}$$

where L_0 and A_0 are, respectively, the original lengths and cross-sectional areas of the component under question, α_L the coefficient of linear expansion, ΔT the change in temperature, F the force due to the pressure in the cell, and E the elastic modulus of the component material. Computed values were compared with analytical approximations for part compression and thermal expansion. At an elevated temperature of 473 K and a pressure of 50 MPa, the lateral deflection of the wafer away from the o-ring due to thermal expansion and compression effects combined is calculated to ~63.5 μm. While this deflection should not compromise the integrity of the o-ring seal, modifications can be made to include more rigid support cylinder materials or materials with more/less thermal expansion as required. The top support cylinder could be fabricated from multiple stacked disks to match the deflection of the steel cell body.

Temperature control is provided by two 25 W Vulcan model C2010 heater cartridges connected to a Lakeshore controller model 340. The heater cartridges (item 8 of Figure 2) are inserted through the cap (3) into 6.35 mm diameter dead-ended holes in the carbon steel top support cylinder (4). Two Pt-100 temperature sensors are inserted into the same cylinder through 1.6 mm holes (sensors are not shown in Figure 2). Both the sensors and cartridges are connected to the temperature controller allowing temperature control to within ±0.1 K.

To prevent scattering of the neutron beam from the steel vessel body two boron nitride masks (Figure 5) were placed in the vessel entrance and exit ports of the NR cell body.

III. PERFORMANCE TESTS OF THE HIGH-PRESSURE CELL

The pressure cell was tested at high pressure to verify the mechanical integrity of the cell and the seal design. The pressure setup, built from High Pressure Equipment Company, Erie, PA (HIP) stainless steel Taper Seal standard parts, is shown in Figure 6. Tubing is 1/16 in. OD stainless steel capillary tubing (HIP) to minimize the total amount of compressed fluid in the system. Prior to use, the setup is flushed with 1,1,2-trichloroethane, ethanol, and acetone to remove contaminants. After cleaning, the entire system is evacuated

Downloaded 06 Apr 2012 to 128.219.49.14. Redistribution subject to AIP license or copyright; see http://rsi.aip.org/about/rights_and_permissions

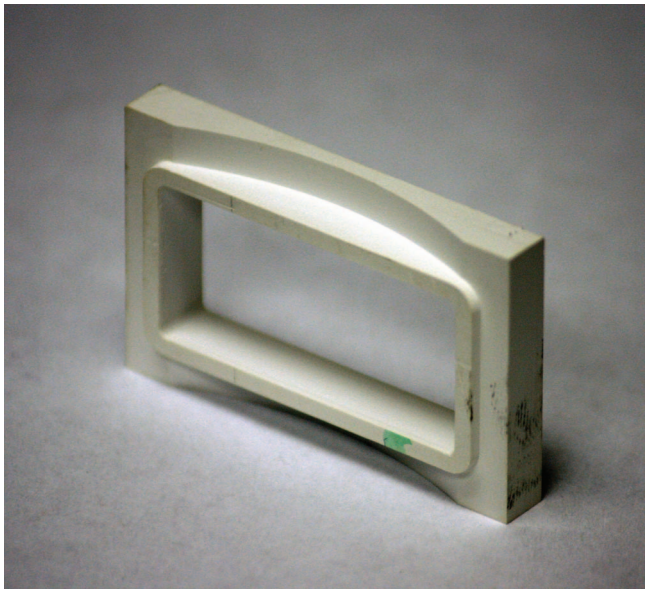

FIG. 5. A photograph of the mask, machined entirely from boron nitride, used to reduce scatter from the steel body prior to entering the wafer.

to a pressure less than 100 Pa (1 mbar) followed by thorough flushing with liquid CO_2 to remove contaminant residues.

The pressure setup, shown in Figure 6, allows independent evacuation of the pressurizer and the high-pressure cell through operation of valve B and use of a portable Adixen AMD 1 oil-free diaphragm vacuum pump. It is designed for fluids that condense at temperatures above 290 K, while fluids that only condense at lower temperatures, i.e., methane, require a different compressor setup. For fluid compression, the valves (B) and (C) are closed and valve (A) opened. Fluid from the bottle enters the cooled piston compressor (C2) (HIP 1 kbar positive displacement pump) and condenses. Valve (A) is then closed and valve (B) opened for pressurization of the high-pressure NR cell (C3). Heat tape can be wrapped around the pressure tubing between Valve B and the high-pressure cell to prevent condensation. The pressure at the high-pressure cell is measured with a Keller high accuracy pressure controller (X33 series), (G2), to better than 10 kPa (0.1 bar). The pressure in the piston pressurizer is monitored through use of a high-precision Keller 0–100 MPa pressure transducer (G1). With valves (B) and (C) closed, the pressure stability has been tested with supercritical CO_2 (T = 50 °C) at 34 MPa (340 bar) for 24 h, during which no measurable pressure loss was detected.

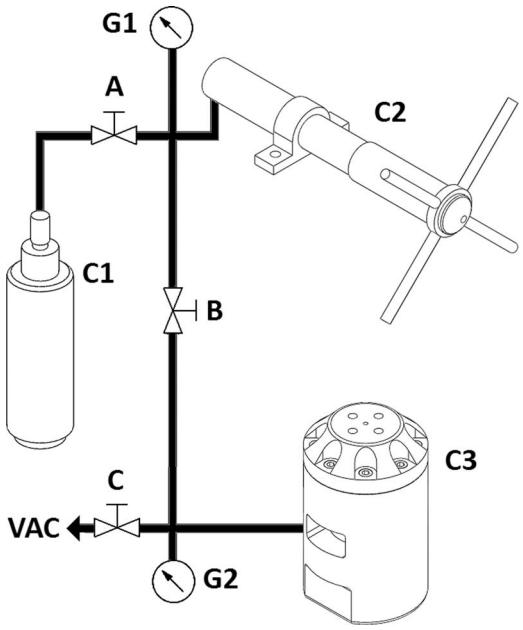

FIG. 6. Schematic of the high pressure fluid delivery system. C1: Bottle with compressed measurement fluid; A, B, C: High pressure needle valves; C2: Piston pressurizer; C3: High-pressure reflectometry cell; G1, G2: pressure gauges; VAC: Oil free vacuum pump.

In order to demonstrate the efficacy of the high-pressure cell, NR measurements were performed on a sample in air and subsequently mounted within the high-pressure cell. The sample was comprised of a thermally grown oxide layer on a Si wafer. Neutron reflectivity measurements were conducted on the Liquids Reflectometer at the SNS at ORNL. Specular reflectivity data were collected using a 3.5 Å bandwidth of neutron wavelength, 2.5 Å $< \lambda <$ 6.0 Å, at seven incident angles θ from 0.15° to 2.80°. With these instrument settings reflectivity data has been acquired covering a wide wave vector transfer ($Q = 4\pi \sin\theta/\lambda$) range of 0.005 Å^{-1} $< Q <$ 0.20 Å^{-1}.

Data from the two measurements were analyzed by simultaneously applying reflectivity profiles derived from a single model scattering length density (SLD) profile. The SLD carries information regarding the composition and density profiles normal to the surface of thin film materials. Model parameters for the SLD profile were adjusted to achieve best fits to each data set (i.e., from air and within the high-pressure cell).

Figure 7 shows the data and the results of the analysis. The upper graph shows reflectivity profiles (solid symbols) as measured for the thermally grown oxide layer on the Si wafer. Black data points correspond to the measurement in air while the red data points to that taken with the sample mounted within the high-pressure cell. The solid lines represent the best fit of the SLD model profile (shown in the bottom graph from air, black line, and within cell, red line) to each data set. As can be seen, a single SLD model represents both data sets well indicating the high-pressure cell does not contribute significant parasitic scattering to the resulting reflectivity profiles. The shape of the SLD profile agrees with the reported data.[14]

An additional high-pressure neutron reflectivity cell has been designed for 2 inch diameter wafers with 10 mm thickness to supplement the existing cell described earlier in this paper while also improving performance. Figure 8 shows a cross-sectional view of this new pressure cell. The wafer (7) thickness in Figure 8 has been increased from 5 mm to 10 mm to improve the signal quality, maximize the angle of scatter, and reduce mechanical stresses on the wafer. A number of additional modifications, described below, were made from the 5 mm cell design to increase temperature homogeneity and simplify cell assembly. To minimize thermal gradients and to achieve a higher maximum temperature, two additional heater cartridges (8) were placed in the support cylinder (6) (not visible in the figure). Items (9), (10), and (11) are fabricated from

Downloaded 06 Apr 2012 to 128.219.49.14. Redistribution subject to AIP license or copyright; see http://rsi.aip.org/about/rights_and_permissions

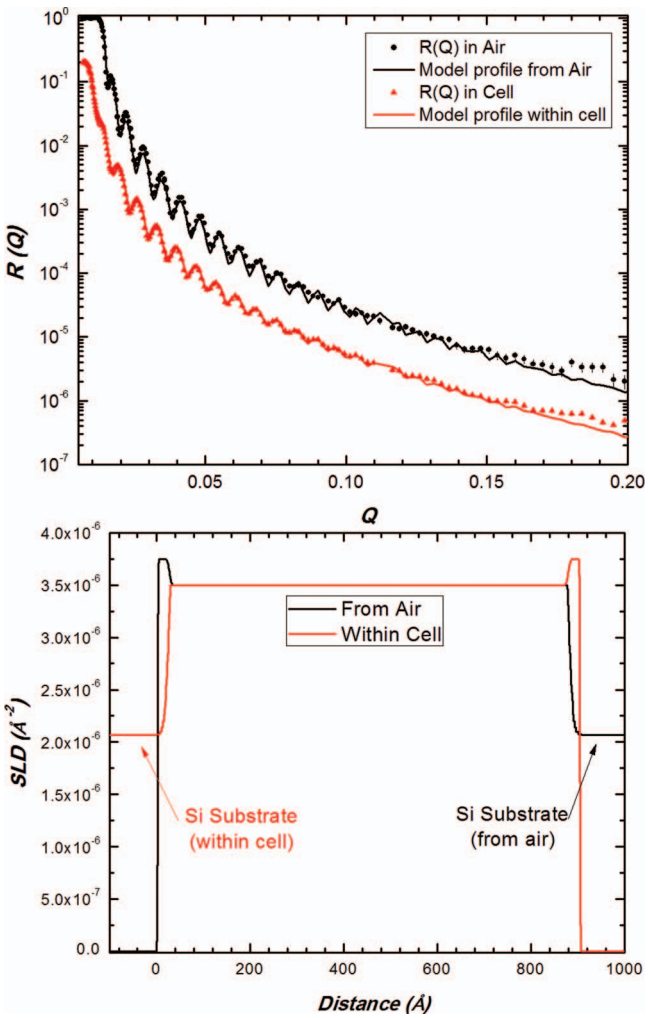

FIG. 7. NR data and analysis of a Si wafer with thermally grown oxide layer. Top: NR curves for measurement in air (black circles) and mounted in the NR pressure cell (red triangles). Data are offset for clarity. Bottom: Plots of the SLD profiles resulting from the NR data obtained in the two measurements.

PTFE and form an insulating jacket to retain the heat in the vessel and reduce thermal inhomogeneity. The upper support cylinder (4) is fastened to the vessel cap (3) to help with alignment and ease of assembly. Two holes drilled into the vessel body (5) allow thermocouples to come directly in contact with the wafer (holes not shown). Lastly, the lower support cylinder (6) was fabricated from both titanium and from a null matrix alloy such as Ti–Zr[15] in an effort to further improve the signal quality.

Tests have shown that at temperature setpoints between 35 °C and 50 °C the thermocouple sensors in the top support cylinder (4) and support cylinder (6) stabilized within 0.01 °C of the set value. The range of high temperature homogeneity can be extended using modern temperature controllers with 2 PID control loops. It was also found that the thicker wafers used in the 10 mm pressure cell have preferential mechanical strength. Wafer cracking under pressure was observed occasionally for Si wafers in the 5 mm cell, but not in the 10 mm cell.

To demonstrate cell functionality at high pressure, two sets of reflectivity curves of supercritical CO_2 adsorbing to crystalline (α-quartz) and amorphous Si/SiO_2 are shown using 10 mm wafers. This experiment was motivated by gravimetric excess sorption data of supercritical CO_2 confined in mesoporous CPG-10, indicating pronounced confinement induced sorption effects on the scale of tens of nanometers.[16] Key questions are how pore confinement and the presence of large surfaces control the pore fluid sorption, and whether their individual impacts on pore fluid properties can be separated. In Ref. 15, large differences in the strength of sorption effects were observed between the two studied pore sizes of 8.1 nm and 31.8 nm. Normalization of the excess sorption to the specific surface area and pore volume indicates that pore confinement controls fluid sorption over a wide range of bulk fluid densities. This finding indicates that the adsorbed layer formed by supercritical fluids at solid interfaces can extend tens of nanometers into the subphase.

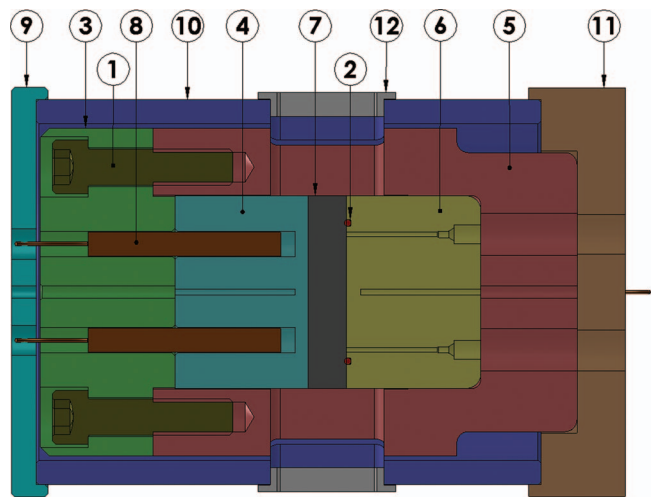

FIG. 8. Cross-sectional view of the pressure cell for wafers with 10 nm thickness. Labels: (1) Pressure retaining fasteners, (2) o-ring seal, (3) pressure cell cap, (4) top support cylinder, (5) high-pressure cell body, (6) support cylinder, (7) wafer, (8) heater cartridges, (9) insulative cap, (10) insulative body, (11) insulative mounting base, and (12) boron nitride masks.

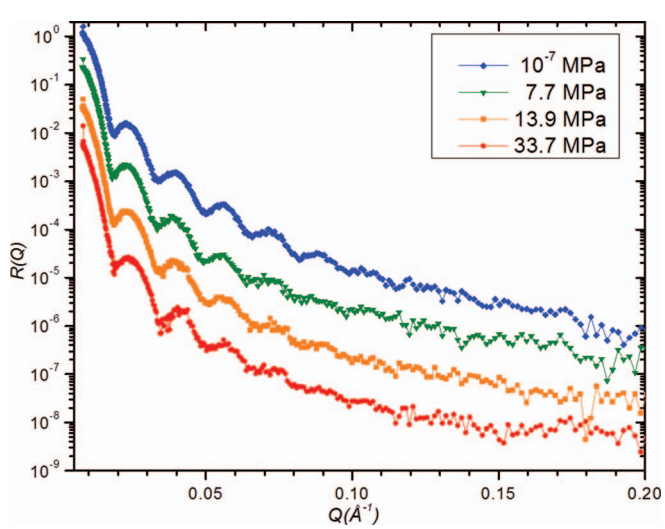

FIG. 9. Neutron reflectivity curves of Si substrate with thermally grown oxide layer in contact with supercritical CO_2 at different pressures and T = 307 K. Data were measured in the 10 mm pressure cell, curves are offset vertically.

Downloaded 06 Apr 2012 to 128.219.49.14. Redistribution subject to AIP license or copyright; see http://rsi.aip.org/about/rights_and_permissions

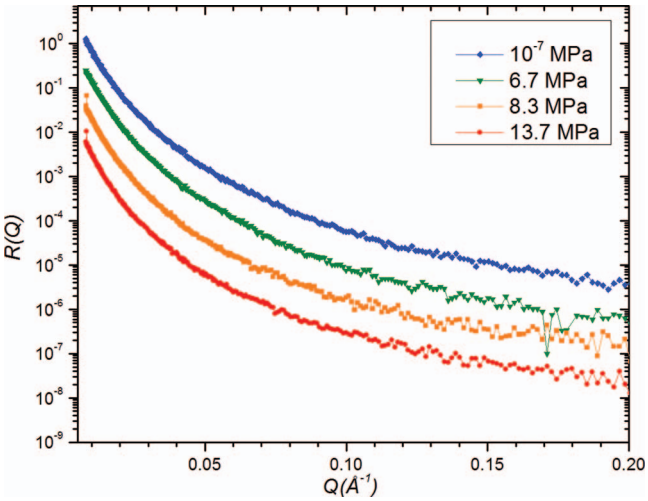

FIG. 10. Reflectivity data of an α-quartz substrate interacting with supercritical CO_2 at various pressures and T = 307 K. Data were measured in the 10 mm pressure cell and are offset vertically.

The fluid density profiles of supercritical fluids formed at flat interfaces with identical chemical composition as the porous solid provide a reference point for studies of confinement effects, but such data have been difficult to obtain experimentally hitherto.

Experimental neutron reflectivity curves for supercritical CO_2 at oxide wafers are shown for a silicon wafer with thick thermally grown layer of amorphous SiO_2 (Fig. 9), and α-quartz (Fig. 10). Data analysis with the goal to extract CO_2 density profiles is currently underway. Initial analysis suggests CO_2 densification at these oxide surfaces, which is in agreement with the gravimetric excess sorption data.[16] The results can be directly compared with MD simulations and may be used to calibrate the solid-fluid interaction potentials used in computer modeling.[17]

IV. CONCLUSIONS

Novel type NR cells accommodating wafers with thicknesses of 5 and 10 mm, respectively, have been built and tested. The main characteristics of the two pressure cells discussed in this paper are the windowless design, and small fluid sample volume of only 0.1 ml. Combined, these design features effectively reduce background scattering, beam distortion, and attenuation. The measurements can be extended to high momentum transfer (approx. 0.3 $Å^{-1}$), which enables high-resolution reflectivity measurements. The cell has been tested in studies of the sorption properties of pure and mixed compressed fluids at mineral surfaces, providing previously unattainable density profiles under sub- and supercritical conditions. A range of other uses is anticipated and the cell is available for use by interested users for their research activities.

ACKNOWLEDGMENTS

Research of G.R., L.M.A., and D.R.C. is based upon work supported as part of the *Center of Nanoscale Control of Geologic CO_2* (NCGC), an Energy Frontier Research Center funded by the U.S. Department of Energy, Office of Science, Office of Basic Energy Sciences under Award Number ERKCC67. A portion of this research at Oak Ridge National Laboratory's Spallation Neutron Source was sponsored by the Scientific User Facilities Division, Office of Basic Energy Sciences, U.S. Department of Energy.

[1] J. B. Hayter, R. R. Highfield, B. J. Pullman, R. K. Thomas, A. I. McMullen, and J. Penfold, J. Chem. Soc., Faraday Trans. 1 **77**, 1437 (1981).
[2] T. P. Russell, Mater. Sci. Rep. **5**, 171 (1991).
[3] C. F. Majkrzak, Acta Phys. Pol. A **96**, 81 (1999).
[4] T. P. DiNoia, C. F. Kirby, J. H. van Zanten, and M. A. McHugh, Macromolecules **33**, 6321 (2000).
[5] J. B. McClain, D. Londono, J. R. Combes, T. J. Romack, D. A. Canelas, D. E. Betts, G. D. Wignall, E. T. Samulski, and J. M. DeSimone, J. Am. Chem. Soc. **118**, 917 (1996).
[6] J. Kohlbrecher, A. Bollhalder, and R. Vavrin, Rev. Sci. Instrum. **78**, 125101 (2007).
[7] I. F. Bailey, Z. Kristallogr. **218**, 84 (2003).
[8] R. R. Gupta, K. A. Lavery, T. J. Francis, J. R. P. Webster, G. S. Smith, T. P. Russell, and J. J. Watkins, Macromolecules **36**, 346 (2003).
[9] S. M. Sirard, R. R. Gupta, T. P. Russell, J. J. Watkins, P. F. Green, and K. P. Johnston, Macromolecules **36**, 3365 (2003).
[10] M. Kreuzer, T. Kaltofen, R. Steitz, B. H. Zehnder, and R. Dahint, Rev. Sci. Instrum. **82**, 023902 (2011).
[11] T. Koga, Y. S. Seo, K. Shin, Y. Zhang, M. H. Rafailovich, J. C. Sokolov, B. Chu, and S. K. Satija, Macromolecules **36**, 5236 (2003).
[12] C. Jeworrek, R. Steitz, C. Czeslik, and R. Winter, Rev. Sci. Instrum. **82**, 025106 (2011).
[13] E. Oberg, F. D. Jones, and H. L. Horton, *Machinery's Handbook* (Industrial Press, Inc., 1976).
[14] A. Athanassouli, Th. Ganetsos, F. Klose, and S. Messoloras, Semicond. Sci. Technol. **17**, 65 (2002).
[15] S. S. Sidhu, L. Heaton, D. D. Zauberis, and F. P. Campos, J. Appl. Phys. **27**, 1040 (1956).
[16] G. Rother, E. G. Krukowski, D. Wallacher, N. Grimm, R. J. Bodnar, and D. R. Cole, J. Phys. Chem. C **116**, 917 (2012).
[17] A. Oleinikova and I. Brovchenko, Phys. Rev. E **78**, 061601 (2008).

Downloaded 06 Apr 2012 to 128.219.49.14. Redistribution subject to AIP license or copyright; see http://rsi.aip.org/about/rights_and_permissions